

Evaluating The Effects of Magnetic Susceptibility
in UXO Discrimination Problems
(SERDP SEED Project UX-1285)

Final Report

Leonard R. Pasion, Stephen D. Billings, and Douglas W. Oldenburg
UBC-Geophysical Inversion Facility
University of British Columbia

David Sinex and Yaoguo Li
Department of Geophysics
Colorado School of Mines

August 4, 2003

Summary of Results

Using numerical simulations based on magnetic susceptibility properties observed at Kaho'olawe, Hawaii, we have examined the effect of magnetic soil on static magnetic method and time-domain electromagnetic (TEM) method in UXO discrimination problems. We have demonstrated that the static magnetic susceptibility can be effectively modeled using a correlated random process, and that Wiener optimal filter can be used as a preprocessing tool to remove the effect of soil response and improve the reliability of dipole inversions. The frequency-dependent susceptibility in TEM method can be modeled using a complex susceptibility having a broad range of relaxation times. A layer of soil with such susceptibility produces the characteristic t^{-1} decay of the voltage measured in TEM at Kaho'olawe. The horizontal component of central loop TEM data is not sensitive to the presence of magnetic soil if it is sufficiently 1D. This provides a preprocessing tool for removing the soil effect from the vertical component data and improving the result of two-dipole inversion. The research project has therefore accomplished the four stated goals of (1) developing and verifying software for simulating soil responses, (2) characterizing the effect of soil susceptibility, (3) determining the applicability of two inversion algorithms, and (4) developing methods for removing the soil effect.

Contents

| | |
|--|----|
| 1. Introduction..... | 4 |
| 2. Response of Magnetic Soils in Magnetic Measurements | 7 |
| 3. Effect of Soil Response on Magnetic Data And Its Removal..... | 14 |
| 4. Effect of Soil Response on TEM Data And Its Removal | 21 |
| 5. The Effect of Magnetic Soils on the Recovery of Dipole Parameters and it removal..... | 30 |
| 6. Conclusions..... | 35 |
| 7. Acknowledgements..... | 36 |
| 8. References..... | 36 |

1. Introduction

1.1 Background

The two most effective geophysical techniques for UXO investigations are magnetic and electromagnetic (time or frequency domain) surveys. These have a well-documented ability to locate UXO's but are prone to excessive false alarms, which significantly increases the cost of clean up. For instance, at some sites up to 75% of excavated items are non-UXO. The key to reducing these false alarms is the development of algorithms that can discriminate between an intact UXO and other items such as scrap metal or geological features.

Recent developments have enabled the recovery of dipole or ellipsoidal parameters through inversion of magnetic data. Additionally, frequency and time-domain electromagnetic measurements can be inverted to recover parameters in reduced modelling formulations. These recovered parameters can be used to discriminate between UXO's and other items. For example, the recovered parameters in a two-dipole model for time-domain electromagnetics can be used to determine whether the object is magnetic (possibly UXO) or not and whether the object is plate-like (non-UXO) or rod-like (UXO).

The above inversion methodologies have been developed with the underlying assumption that the collected data result from objects buried in a very resistive and non-magnetic background. In practice this is not always the case. At many sites (e.g. former Fort Ord; the former Naval range at Kaho'olawe, and Helena Valley, Montana) the soils are known to have significant magnetic susceptibilities. That background significantly modifies the measured magnetic or electromagnetic responses and thus adversely affects the performance of the existing inversion algorithms. This reduces our ability to discriminate and results in false alarms. For instance, approximately 60,000 anomalies were dug at Kaho'olawe site, and the false-alarm rate is about 32 to 33. Among the false anomalies, 70.3% were caused by non-hazardous metal objects and 27% were caused by geology. Therefore, it is important that we understand the effect of magnet soil on these two widely used techniques in UXO detection and discrimination and develop

approaches to mitigate such effect in order to improve the detection and discrimination capabilities.

The purpose of this project is therefore to determine how magnetic soils affect the recovered parameters from magnetic and electromagnetic (EM) inversions and, if this effect is significant, to explore possible techniques to mitigate their effects. The specific objectives are:

- (1) Quantitatively evaluate the effects of the background susceptibility and thereby determine under what conditions our inversion algorithms can work (while ignoring these effects),
- (2) Determine how the data can be modified so that the current inversion algorithms will work in the presence of background susceptibility.

In this report, we will provide a brief background on the factors that affect the soil susceptibility and then study the response of soil magnetic susceptibility in static magnetic and in time-domain electromagnetic surveys, and assess the level of soil response that will severely affect the performance of current discrimination algorithms based on geophysical inversion. Preliminary methods for removing the effect of background response are also developed.

1.2 Soil Magnetic Susceptibility

The task of discriminating UXO from non-UXO items is more difficult when sensor data is contaminated with geological noise originating from magnetic soils. The magnetic properties of soils are mainly due to the presence of iron. Hydrated iron oxides such as muscovite, dolomite, lepidocrocite, and goethite are weakly paramagnetic, and play a minor role in determining the magnetic character of the soil. The magnetic character of the soil is dominated by the presence of ferrimagnetic minerals such as maghaemite and magnetite. Maghaemite is considered the most important of the minerals within archaeological remote sensing circles (e.g., Scollar et al., 1990). Magnetite is the most magnetic of the iron oxides, and is the most important mineral when considering the effects of magnetic soils on total-field magnetic and EM measurements.

Given the presence of these magnetic minerals, the strength of the magnetic susceptibility and its behavior are determined primarily by two factors. The first is the mass fraction of the dominant magnetic minerals. The more abundant these magnetic minerals are in the soil, the higher the magnetic susceptibility values are. The second is the grain size distribution within the soil. Very small grains have very short, almost instantaneous relaxation times, while large grains have multiple grains and are stable. Some single domain grains can exist in a stable state, but often they may exhibit a range of relaxation times.

The magnetic soil at Kaho’olawe site has been studied by other researchers and we cite the data here as examples of the frequency-dependent susceptibility. The magnitude of the susceptibility value also provides the basis for our simulation of soil response in the later sections. Kaho’olawe is a single volcanic dome made of thin bedded pahoehoe and a’ a basalt (Stearns,1940). Base rock is tholeiitic basalt (Butler, personal communication) and it is covered by a number of different soil types with variable geophysical characteristics (Parsons-UXB,1998). As examples, Tables 1 lists the magnetic susceptibilities measured at a site on Kaho’olawe. The susceptibility varies over a large range and it attains a decreased value at the higher frequency.

Table 1. Magnetic susceptibilities of four samples collected at Seagull site on Kaho’olawe. The susceptibility is measured at two frequencies and the unit is 10^{-5} SI.

| Sample - depth | Frequency (0.46 kHz) | Frequency (4.6 kHz) |
|----------------|----------------------|---------------------|
| A-6" | 3554 | 3344 |
| A-24" | 3022 | 2771 |
| AP-6" | 1726 | 1630 |
| AP-18" | 1529 | 1448 |

The static magnetic sensors are sensitive to the presence of magnetic minerals because the earth’s magnetic field creates an induced magnetization. The anomalous magnetic field produced by the soil magnetization will superimpose on the magnetic anomalies produced by UXO’s and other metallic objects and therefore introduce adverse effect in the discrimination problem.

Electromagnetic sensors are sensitive to the presence of magnetite due to the phenomenon of magnetic viscosity. Electromagnetic sensors illuminate the subsurface with a time or frequency varying primary field. Suppose that we apply a magnetic field to an area containing magnetic soil, the magnetization vector of the soils will try to adjust to align itself with the exciting field. At the instant the magnetic field is applied there is an immediate change in magnetization and, possibly, an additional time dependent change in magnetization. This time dependent phenomenon is referred to as magnetic viscosity or magnetic after-effect. A time constant is used to characterize the time for the magnetization vector to rotate from its minimum energy orientation prior to application of the field, to its new orientation. The time-dependent magnetization creates time-varying magnetic field that will be superimposed on the time-varying field due to the decaying electric current in a UXO.

In the following, we first investigate the effect of magnetic soil on static magnetic measurements by simulate magnetic soil using correlated random susceptibility distributions and quantify the errors it introduces to the inversion. We then investigate the effect of viscous magnetic soil on TEM data and show that the $1/t$ decay in TEM data is caused by the presence of complex susceptibility. In both cases, we develop methods to remove the soil response before applying inversion algorithms for discrimination.

2. Response of Magnetic Soils in Magnetic Measurements

2.1 Simulation of Soil Magnetic Susceptibility

To evaluate the effect of magnetic soil on the total magnetic intensity (TMI) measurements in UXO detection and discrimination, we assume a general model of susceptibility distribution without too much site-specific information. We represent the 3D susceptibility variation by a 3D grid of cells typically of cubic shape. Given the non-deterministic nature of the soil physical property, we choose to use a correlated random process to represent the spatial distribution of susceptibility. Such a process can be modeled by a power spectrum that decays with the spatial wavenumber and has a random phase term (e.g., Easley et al. 1990 and Shive et al. 1990).

Let $\chi(x, y, z)$ be the magnetic susceptibility in the 3D volume of subsurface to be modeled, and $P(\omega_x, \omega_y, \omega_z)$ be its power spectrum, where $(\omega_x, \omega_y, \omega_z)$ are respectively wavenumbers in the x-, y-, and z-directions. Then the 3D Fourier transform of the susceptibility is given by

$$\tilde{\chi}(\omega_x, \omega_y, \omega_z) = \sqrt{P(\omega_x, \omega_y, \omega_z)} e^{-i\phi(\omega_x, \omega_y, \omega_z)}, \quad (1)$$

where $\phi(\omega_x, \omega_y, \omega_z)$ is the phase term. Given a power spectrum, we can simulate different realizations of the random process by assigning different random phases. All realizations would have the same power spectrum, and thus have more or less the same appearance in the space domain. However, the locations of features seen in each realization will be different.

In practice, it is often easier to estimate a radially averaged power spectrum than a 3D spectrum. For this study, we assume a radial power spectrum of the form

$$P(\omega_r) = [1 + (\omega_r / \omega_0)^2]^{-\beta}, \quad (2)$$

where $\omega_r = \sqrt{\omega_x^2 + \omega_y^2 + \omega_z^2}$ and ω_0 is a cutoff frequency and it's inversely proportional to the correlation length of the random process. The parameter β determines how fast the spectrum decays with wavenumber and, thus, how correlated the process is. A value of $\beta = 0$ produces a flat power spectrum and corresponds to an uncorrelated random process. Figure 1 displays an example of such a radial power spectrum with $\beta > 0$.

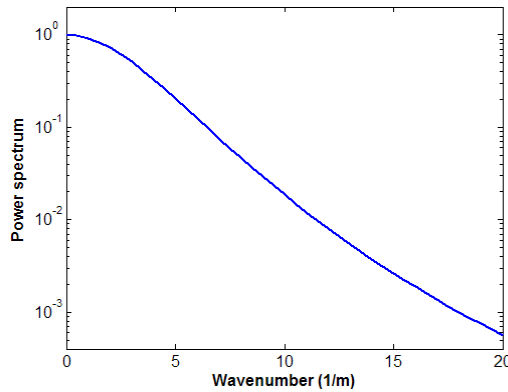


Figure 1 An example radial power spectrum described by eq.(1).

To generate the Fourier transform of susceptibility, the last step is to assign values to the phase term. Since the phase is essentially limited to the range of $[0, 2\pi]$, we choose to assign the value as uniformly distributed between $[0, 2\pi]$. Once the Fourier transform of the susceptibility is constructed according to eq.(1), applying inverse transformation yields a susceptibility model in the 3D subsurface volume. The model is then scaled and shifted in DC value to produce a desired susceptibility model with a prescribed mean and standard deviation. Figure 2 displays an example susceptibility model produced by this procedure. Note that the highs and lows of the susceptibility value appear to be randomly located, yet they also occur in blotches with a certain length scale.

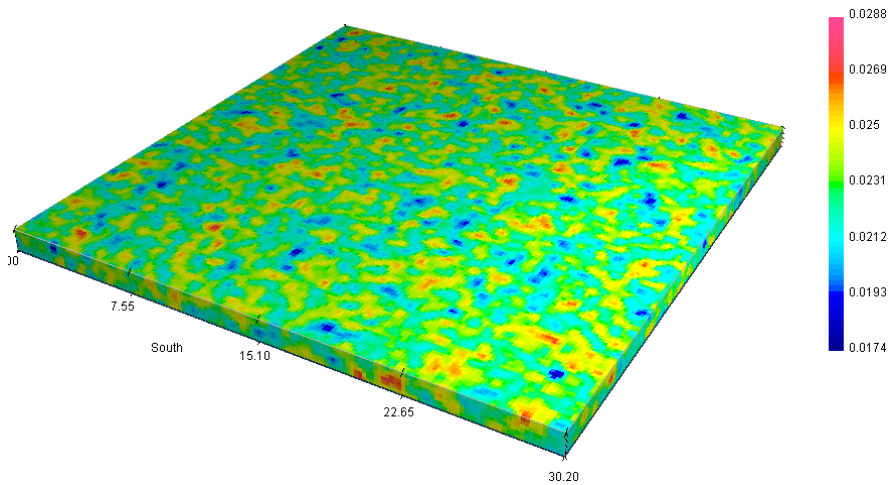


Figure 2 An example of correlated random susceptibility generated by the procedure described in this section. Note that the highs and lows of the susceptibility value appear to be randomly located, yet they also occur in blotches with a certain length scale.

2.2 Estimating Parameters for Correlated Random Susceptibility

The preceding section describes a general procedure for generating susceptibility models that can be used in simulating the response of magnetic soils. For meaningful practical applications, we must estimate the defining parameters ω_0 and β , as well as the amplitude of the susceptibility. These parameters will be site-dependent. For the current study, we have chosen to use information from the Kaho'olawe, Hawaii, where we estimate the power spectral parameters

from TEM data and determine the strength of the susceptibility based on the measured values from soil and rock samples.

A set of EM63 data was acquired at the site. Most data located away from buried metal targets exhibit a $1/t$ decay because of the magnetic viscosity of the top soil at the site. The details of the analysis of these TEM data will be presented in a later section of this report. The pertinent result for this portion of the research is that the strength of the $1/t$ decaying voltage is proportional to the strength of the magnetic susceptibility at the location of TEM measurement. Plotting the scaling factor A derived from fitting the function A/t to each TEM curve yields the spatial variability of the susceptibility in the horizontal directions. Figure 3 displays a subset of quantity derived at Kaho'olawe site. In order to prepare the TEM data for analysis, all the anomalies due to UXO and non-hazardous metal objects were removed, leaving only variations in the data that are due to geology. The data were gridded using a minimum curvature technique. The holes were filled in by interpolation. A second order trend is removed to accentuate the short-wavelength variations that are of interest to this study. We note that this map has a random appearance similar to that in Figure 2, but there are also long-wavelength variations.

Taking the 2D Fourier transform of the data and calculating the radially averaged power spectrum yields an estimated radial power spectrum of the data set. We then perform a least-squares fit to the functional form in eq.(1) to determine the parameters ω_0 and β . The result is shown in Figure 4 and the values of the two parameters are $\omega_0 = 2.5$ and $\beta = 1.8$. These values are then assumed to be representative of the spectral property of the soil magnetic susceptibility in 3D at Kaho'olawe site, and we will use them in the subsequent simulations.

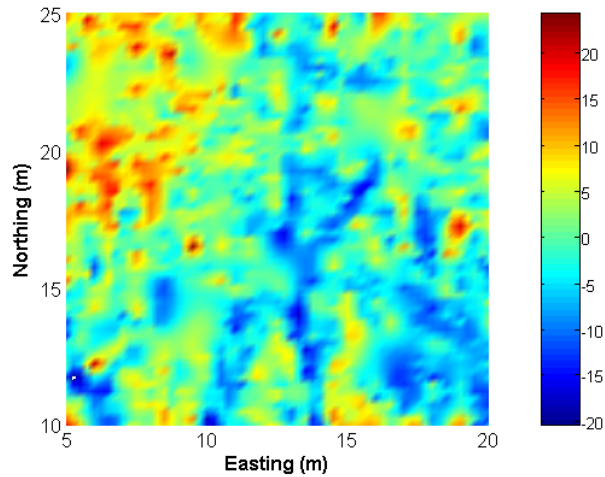


Figure 3 Spatial distribution of magnetic susceptibility at Kaho'olawe , Hawaii. The color image is the strength of $1/t$ decay of measured TEM data and it is directly proportional to the magnetic susceptibility.

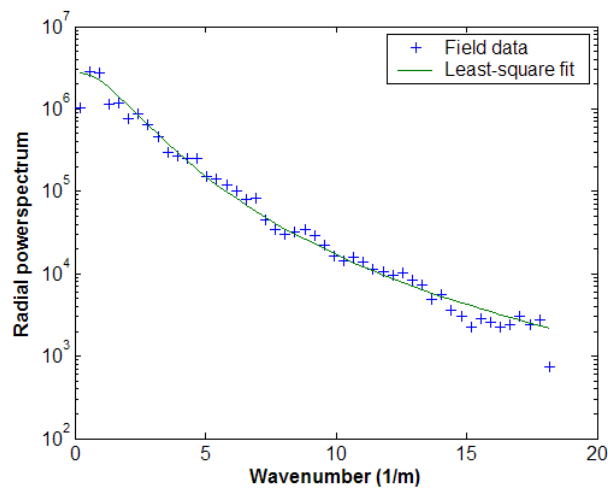


Figure 4 Estimated radial power spectrum. The pluses (+) are the radially averaged power spectrum of the data shown in Figure 3, and the solid line is the result of least-squares fitting to the functional form in eq.(2).

2.3 Simulated Soil Response

We now begin simulating the response of magnetic soil using the parameters estimated at Kaho'olawe. We adopt a model shown in Figure 5. Background geology is assumed to consist of a 1-m layer of soil overlying a half-space of base rock. Without any loss of generality, we

assume the susceptibility of base rock is zero. Since it is unweathered and the susceptibility is either constant or varies very slowly. Such a susceptibility variation only produces a constant shift or long-wavelength variations in the measured magnetic data on the surface, which can be easily taken into account in an inversion. Thus a zero-susceptibility assumption is valid. The layer has a thickness of 1 m and emulates the weathering layer present at Kaho’olawe site that has spatially variable susceptibility. We generate the susceptibility within the layer using the correlated random process based on the spectral parameters estimated in the preceding section and a magnitude consistent with that of measured values of rock samples. The dipole representing a UXO is buried at different depth and have a dipole moment of 0.5 Am^2 . In addition, we assume a sensor height of 0.5 m above the ground. The response of simulated soil is calculated by summing the magnetic fields produced by individual cubic cells (e.g., Sharma, 1966; Li and Oldenburg, 1996). The dipole field is calculated using the standard dipole field formula (e.g., Blakely, 1995).

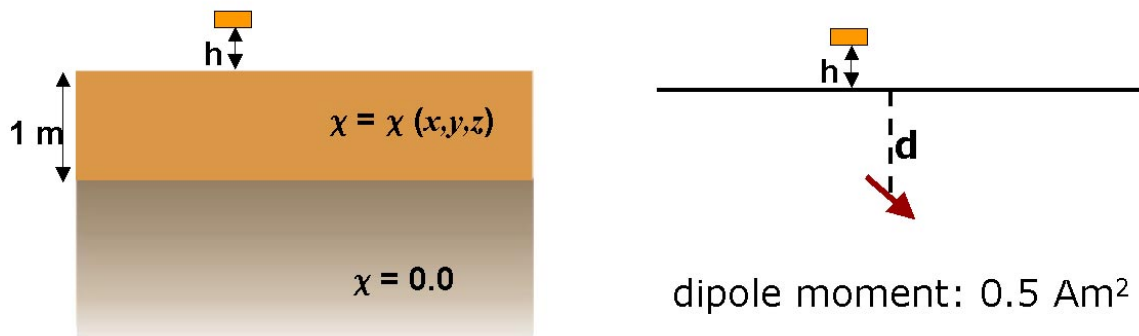


Figure 5 Theoretical model for examining the effect of soil magnetic susceptibility on total magnetic intensity (TMI) data.

Figure 6 shows an example of the soil response. The susceptibility in the layer has a mean value of 0.7 SI and the dipole is at a depth of 0.6 m. Panel (a) displays the magnetic anomaly produced by the simulated soil. Panel (b) is the dipole anomaly. The anomalies in the soil response have a length scale comparable to that of the dipole anomaly. Sum of the two is given in panel (c). The dipole anomaly is clearly visible in this case but there are also other highs and lows caused by

the soil. We can expect that the presence of these highs and lows will lead to large errors in the recovery of dipole parameters through the inversion, which in turn causes difficulties in discrimination.

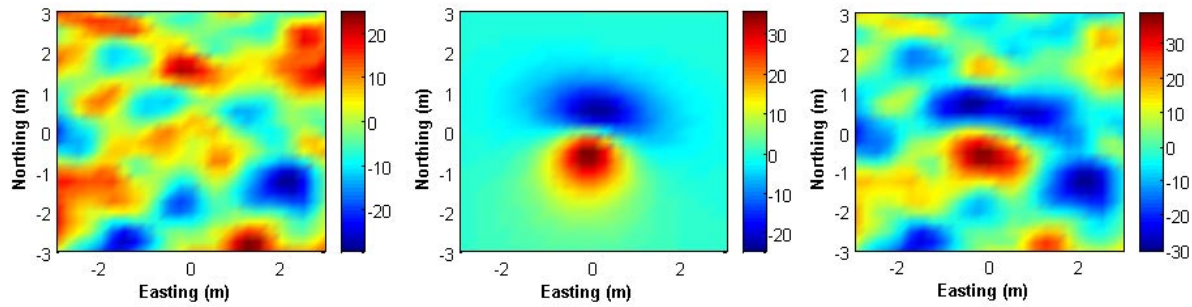


Figure 6 Example response of the soil layer with variable susceptibility and a buried dipole. The dipole is buried at a depth of 0.6 m and the layer has a mean susceptibility value of 0.07 SI.

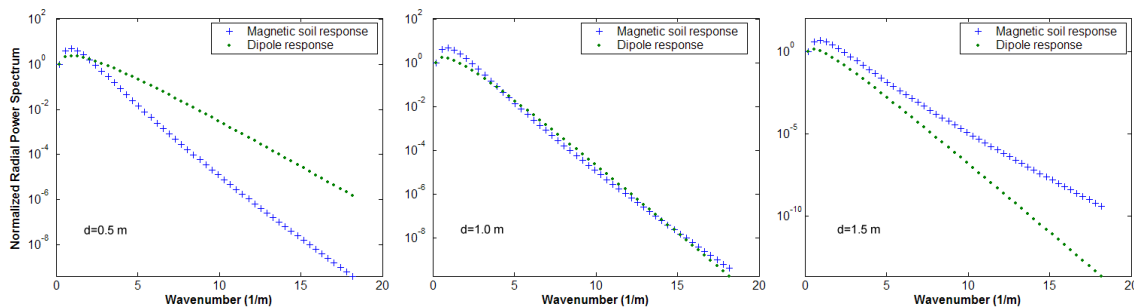


Figure 7 Comparison of the radial power spectra of the magnetic field due to a buried dipole (dots) at different depth and due to a 1-m susceptible layer (pluses). All spectra are normalized for comparison. The dipole depth is indicated in each panel. Soil response has the same frequency content as that of a dipole at 1-m depth. Assuming the same magnitude of responses, UXO responses will only be visible when it is buried above that depth.

Before proceeding to a systematic evaluation on the effect of soil susceptibility, we first develop a qualitative criterion to determine under what conditions the dipole anomaly might be visible in the background soil responses. This can be achieved by examining the power spectra of the two anomalies. Given the assumed parameters of the variable-susceptibility layer and that of the dipole, we can derive the radial power spectrum of the magnetic field produced by either source

(Blakely, 1995). For simplicity, We can consider the spectrum of the magnetic anomaly produced by a single layer of cubic cells at the surface of the earth since this layer has the broadest power spectrum. According to Blakely (1995), the power spectrum is given by

$$P_{layer} \propto [1 + (\omega_p / \omega_0)^2]^{-\beta} e^{-2\omega_p h} (1 - e^{-\omega_p \Delta z}), \quad (3)$$

where ω_p is the radial wavenumber in 2D, h is the sensor height and Δz is the cell thickness. The power spectrum of the magnetic field produced by a dipole is given by

$$P_{dipole} \propto \omega_p^2 e^{-2(h+d)\omega_p}, \quad (4)$$

where d is the depth of burial of the dipole. Assuming the spectral parameter ω_0 and β from the above estimation and the sensor height of $h = 0.5$ m, we can compare the two radial power spectra for different dipole depths. Figure 7 displays the normalized power spectra assuming three different dipole depths.

At a half-meter depth, the power spectrum of the UXO response is above that of the soil response. Therefore, we have enough high-frequency content in UXO response for it to be detected. When the depth increases to one meter, the two power spectra have the similar relative shape, that means given high enough soil magnetic susceptibility, we can no longer distinguish between the anomalies produced by the two different sources. Further increasing the dipole depth means that soil response will completely mask the UXO response since the power spectrum of soil response has much more higher frequency contents. It follows that, given the spectral property at Kaho'olawe, if the UXO anomaly and soil response have comparable magnitude, UXO's can only detected directly using magnetic data if they are buries at a depth shallower than 1.0 m.

3. Effect of Soil Response on Magnetic Data And Its Removal

3.1 Effects of Soil Response on Inverted Dipole Parameters

One of effective UXO discrimination algorithms currently available is based on the magnetic dipole moment recovered from the inversion of surface total-field magnetic anomaly (Billings *et al.*, 2002). In this algorithm, the surface magnetic data measured in the field are inverted to

recover six dipole parameters $\vec{m}_{mag} = (x, y, z, m_x, m_y, m_z)$ that define the dipole moment, direction, and position. The direction or its deviation from the current earth field is then used to discriminate between UXO and scrap metals. The magnitude of the dipole moment is then used to derive a minimum remanent magnetization for the purpose of classification. Reliable recovery of these parameters is crucial to the success of the algorithm. The anomalies produced by susceptible soil can adversely affect the inversion and there hinder the discrimination capability. It is therefore important to quantify the errors caused by the presence of magnetic soil.

To examine the effect, we invert the dipole magnetic data contaminated by soil response and calculate the errors by comparing the recovered dipole parameters with their true values. We carry out this process for different combinations of magnetic susceptibility strengths and dipole depths. The dipole moment is assumed to be 0.5 Am^2 . This value is based on the dipole moments recovered from the application of the discrimination algorithm to active clearance sites (Billings *et al.*, 2002). The mean susceptibility value ranges from 0.01 to 0.1 in 0.01 increment, and the dipole depth ranges from 0.1 m to 1.2 m in 0.1-m increment. The result is a measure of the error as a function of dipole depth and soil susceptibility. To ensure the reliability of the error estimate, we generate 20 different realizations of the correlated random susceptibility. Thus for each combination of the susceptibility strength and dipole depth, we invert 20 data sets to obtain 20 different recoveries of the dipole parameters. A mean and standard deviation are calculated for the error. The results are detailed in the following.

Figure 8 shows the errors for the recovered dipole position. The panel on the left shows the RMS error in the recovered dipole position and the one on the right shows the standard deviation. The horizontal axis is the true dipole depth and the vertical axis indicates the amplitude of soil susceptibility denoted by its mean value. As discussed above, each point in the map is calculated from 20 different sets of inverted dipole parameters. The error increases with both the dipole depth and amplitude of soil susceptibility. Figure 9 shows the errors for the recovered dipole moment. Figure 10 displays the errors in the recovered dipole direction. There is a similar pattern of large errors with increased soil susceptibility and dipole depth in all three figures. This is expected since an increase in either soil susceptibility or dipole will decrease the relative strength

of the dipole response compared to the soil response and therefore lead to large errors in the inversion.

These error maps provide a quantitative indicator by which one can assess the viability of using magnetic data in discrimination. For example, assuming the soil at a site has a similar spectral property as that in Kaho’olawe, we would not expect magnetic method to be effective if the soil susceptibility is above 0.07 SI. Above this level, both dipole moment and direction recovered from inversion will have too large an error to be useful. Similarly, if the UXO is buried deeper than 1.0 m, even a moderately magnetic soil will mask the dipole response and render the inversion unusable. The results presented here assume a dipole moment of 0.5 Am^2 . If the dipole moment is smaller, the above-mentioned threshold of soil susceptibility and dipole depth will decrease since the amplitude of the dipole response will decrease proportionally. A new set of simulation should be performed accordingly.

In general if the combination of the soil susceptibility strength and UXO depth falls within the upper right triangular region of the plots in Figures 8-10, direct inversion of magnetic data for UXO discrimination will be ineffective. In such cases, preprocessing of the data to remove the effect of soil response is required. We present one approach in the following.

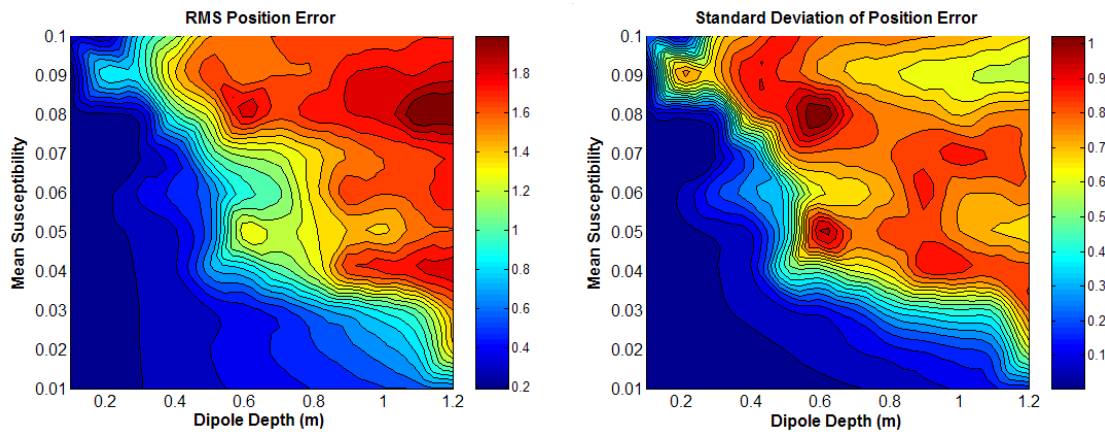


Figure 8 Root mean squared (RMS) error and standard deviation of the position of the recovered dipole position. The error is measured as the distance from the true position of the dipole.

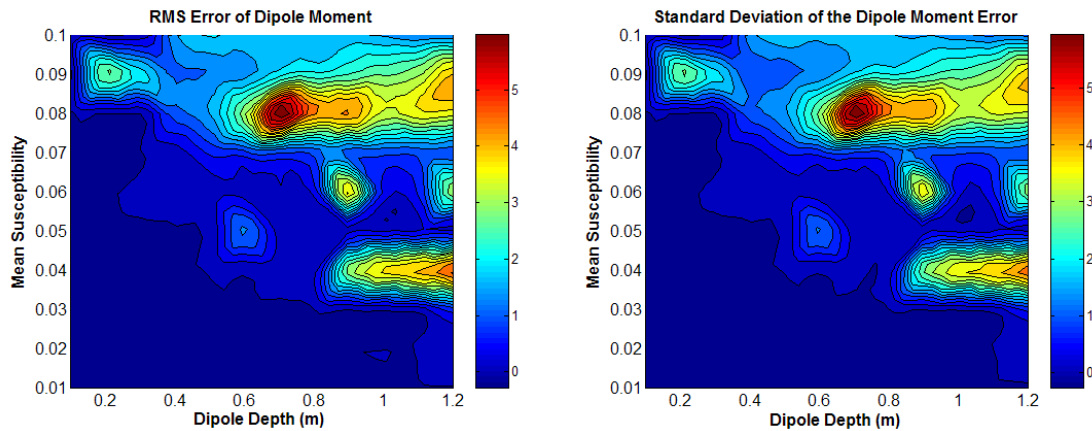


Figure 9 RMS error and standard deviation of the recovered dipole moment. The error is measured as the difference between the recovered and true dipole moment.

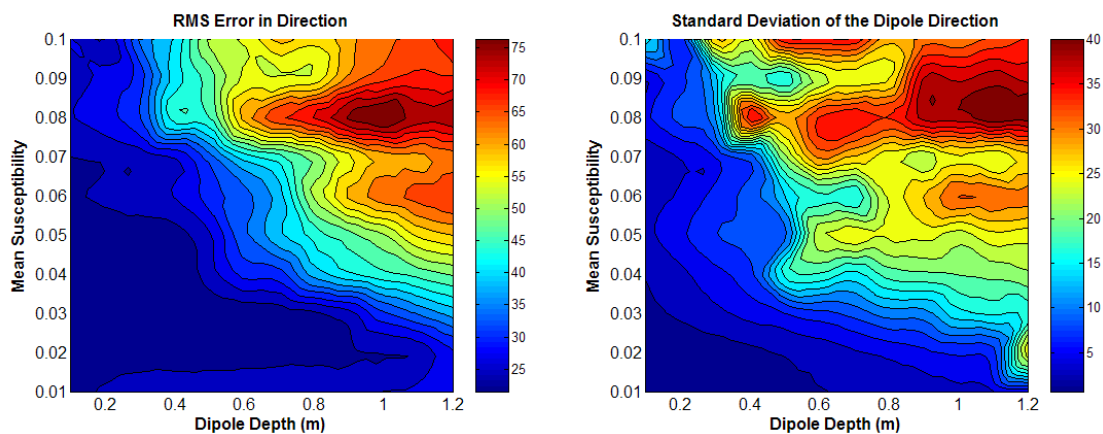


Figure 10 RMS error and standard deviation of the recovered dipole direction. The error is measured as the angle in 3D space between the recovered and true dipole direction. The color scales both indicate angles in degree.

3.2 Removal of Soil Response From Magnetic Data

Like most geophysical inversion, the algorithm for recovering magnetic dipole parameters assumes that the noise in the data is uncorrelated. When this assumption is met, the inversion can separate the signal from noise to a large extent. Difficulty arises when the noise is correlated.

Then the noise has the appearance of signal and cannot be easily separated by the inversion algorithm. Such is the case when we have correlated random susceptibility in the soil surrounding a UXO. The anomalies produced by the soil have features similar to that of UXO anomalies. Preprocessing is then required to remove as much noise as possible prior to inversion. Here we propose to use Wiener filter to accomplish this.

Wiener (1949) filter was developed in communication theory to extract a signal from data that are contaminated by noise. This is a Fourier-domain filter defined by the power spectra of different components in the data. Wiener filter assumes there are two components, namely signal and noise, in the data and constructs a transfer function in the Fourier domain such that the filtered data is closest to the desired signal in the least squares sense. Let $Y(\omega_x, \omega_y)$ be the transfer function, $\tilde{B}_{obs}(\omega_x, \omega_y)$ be the Fourier transform of the magnetic data consisting of the dipole and soil responses, the desired dipole response $\tilde{B}_{dipole}(\omega_x, \omega_y)$ extracted from the data is given by,

$$\tilde{B}_{dipole} = Y * \tilde{B}_{obs}. \quad (5)$$

The transform function is defined by the ratio of two power spectra:

$$Y(\omega_x, \omega_y) = \frac{P_{dipole}}{P_{obs}}, \quad (6)$$

where P_{dipole} is the power spectrum of the dipole response and P_{obs} is the power spectrum of the data. The assumption leading eq.(6) is that the signal (dipole response) and noise (soil response) are not correlated. For practical applications, this filter works well even the assumption is only weakly valid. The key is to have reliable estimate of the power spectra.

In practice, we do not know the power spectrum of the dipole response, which is the quantity we are seeking to extract. However, we can calculate the power spectrum of the observed data and estimate a power spectrum of the soil response by using data that are clearly not affected by UXO responses. Based on the assumption that the soil and dipole responses are not correlated, we can approximate the dipole power spectrum by the difference between the data and soil power spectra. This yields an approximate transfer function that is commonly used to replace the idealized transfer function in eq.(4):

$$Y(\omega_x, \omega_y) \approx \frac{\bar{P}_{obs} - \bar{P}_{soil}}{\bar{P}_{obs}}. \quad (7)$$

As an illustration, we apply this filter to a set of severely contaminated data that were generated using the simulated soil and dipole model. The result is shown in Figure 11. The two top panels show respectively the soil and dipole responses. The soil layer has the same spectral property as before, and the mean susceptibility value is 0.07. The dipole is buried at a depth 1.0 m. Figure 11(c) displays the superposition of the two, which simulates the data contaminated by soil responses. There is little visual indication of the presence of a dipole anomaly. This is expected because this combination of soil susceptibility and dipole depth is well within the zone of large inversion errors in Figure 8-10. Figure 11(d) is the result obtained by applying Wiener filter. The data power spectrum is estimated from the Fourier transform of the data, and the power spectrum of the soil response is estimated from the data in Figure 11(a). We can see that now a dipole anomaly is clearly visible. Inversion of the processed data is also expected to produce much better results.

This is demonstrated by the results shown in Table 3, which compares the dipole moment (m) and dipole direction (declination D and inclination I) recovered from inverting the raw data in Figure 11(c) and the processed data in Figure 11(d). The second column lists the true values of these parameters. The third lists the values recovered from the raw data. There are large errors. The fourth column lists the improved results obtained from inverting the preprocessed data and they are much improved.

3.3 Summary

Wiener filter is effective in suppressing the soil response. However, its effectiveness depends critically on our ability to estimate the power spectrum of the soil response. In general, we can be confident that the filtered result will be useful for detection purposes, but it may not be sufficient for discrimination purposes. Reliable estimation of the power spectrum of soil response depends on good characterization of spatial variation of susceptibility at the clearance site. Further work using field data at sites with strong magnetic soil is therefore required.

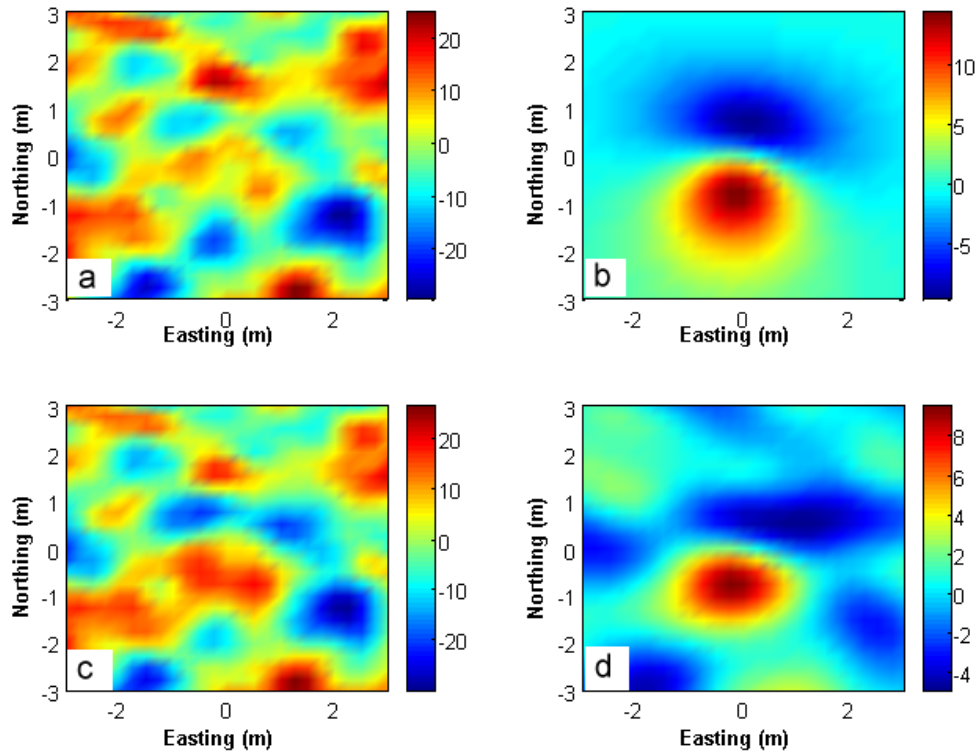


Figure 11 Example of Wiener filtering applied to remove the effect of soil responses. Top panels show respectively the magnetic data generated by the soil with a mean value of 0.07 SI and a dipole at a depth 1.0 m. Lower left panel is the superposition of the two, and lower right panel is the extracted dipole response by using the Wiener filtering.

Table 2 Comparison of the true dipole parameter with those recovered from soil contaminated data and from Wiener filtered data. In the table, m denotes the dipole moment, D is the declination of the dipole direction and I is the inclination.

| | Real Value | With Soil Response | Wiener Filtered Data |
|-----|------------|--------------------|----------------------|
| m | 0.5 | 1.8 | 0.2 |
| D | 9.8 | 10.0 | 11.7 |
| I | 36.2 | -11.6 | 27.9 |

4. Effect of Soil Response on TEM Data And Its Removal

4.1 Frequency Dependent Susceptibility Models

Lee (1983) showed for that a sample containing a collection of particles with a uniform distribution of decay times has a magnetic susceptibility of

$$\chi = \chi_o \left[1 - \frac{1}{\ln(\tau_2 / \tau_1)} \ln \left(\frac{i\omega\tau_2 + 1}{i\omega\tau_1 + 1} \right) \right] . \quad (8)$$

This model of susceptibility is expressed as a function of two time constants (τ_1 and τ_2) that determine the limits of the uniform distribution of time constants, and the static ($\omega=0$) susceptibility χ_o . The quadrature and inphase components described by this model are plotted in Figure 12(a). Between the frequencies $\omega=1/\tau_2$ and $\omega=1/\tau_1$ the quadrature component of susceptibility is nearly constant, but there is a peak at $\omega_m=(\tau_1 \tau_2)^{-1}$. The inphase component decreases linearly with the logarithm of frequency.

The Cole-Cole model has also been used to represent the magnetic susceptibility (for example (Olhoeft and Strangway, 1974; and Dabas et al., 1992). Figure 12(b) contains plots of the Cole-Cole distribution for a range of distributions. The Cole-Cole model for magnetic susceptibility is:

$$\chi = \chi_\infty + \frac{\chi_o - \chi_\infty}{1 + (i\omega\tau)^{1-\alpha}} \quad (9)$$

where χ_∞ is the real susceptibility as frequency approaches infinity ($\omega \rightarrow \infty$) and χ_o is the real susceptibility as frequency approaches zero ($\omega \rightarrow 0$). We assume that $\chi_\infty = 0$ and that the model for magnetic susceptibility can be written as

$$\chi = \frac{\chi_0}{1 + (i\omega\tau)^{1-\alpha}} \quad (10)$$

The parameter α is related to the distribution of relaxation times. The limits of α are $\alpha=0$ for a single Debye relaxation mechanism (Olhoeft and Strangway, 1974) and $\alpha = 1$ for an infinitely broad distribution of relaxation times. A plot of Cole-Cole distributions for a range of α values is shown in Figure 12.

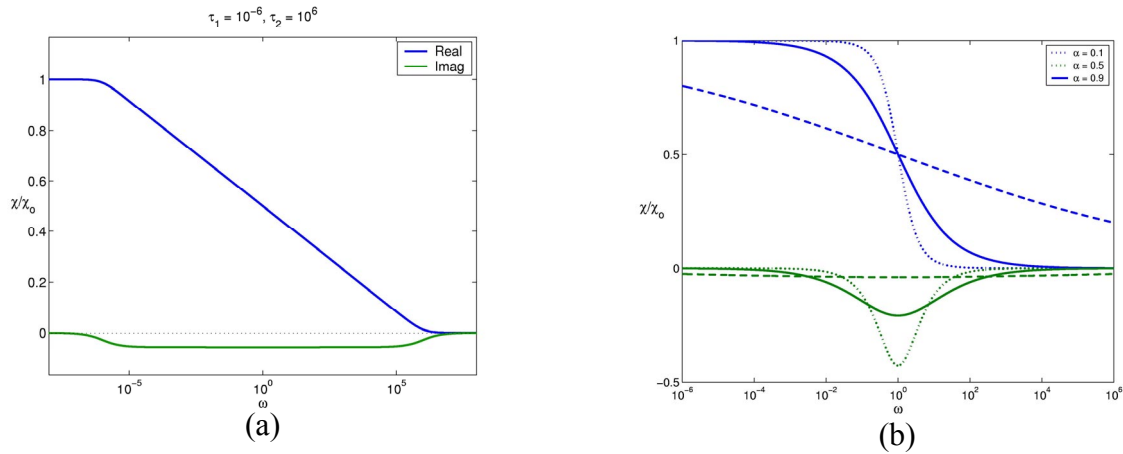


Figure 12 Different frequency dependent susceptibility models. Panel (a) shows the susceptibility model from Lee (1983), and panel (b) shows Cole-Cole model of susceptibility as a function of α . The time constant is $\tau=1$.

For the broad range of distribution of relaxation times that we are assuming in this study, we would expect to model susceptibility with α values approaching 1. The time constant τ controls the location of the peak of the imaginary part of the susceptibility, with the peak occurring at $\omega=1/\tau$. For large α the Cole-Cole model yields a straight line for the real part and a constant negative value for the imaginary part. This is the same as Lee's representation and is a key characteristic for determining the behaviour of the electromagnetic response.

4.2 Constructing a Magnetic Susceptibility Model from Kaho'olawe Soil Measurements

The problems of magnetic soils at Kaho'olawe have been well documented (Cespedes, 2001). A model for the frequency dependent susceptibility of Kaho'olawe soils is required to investigate Kaho'olawe is a single volcanic dome made of thin bedded pahoehoe (smooth, very fast moving

lava) and 'a'a (rugged, slow moving lava) basalt (Stearns, 1940). The base rock is tholeiitic basalt, containing up to 20% magnetite (Butler, personal communication, 2001). The base rock is covered by a number of different soil types with variable geophysical characteristics (Parsons-UXB, 1998). For clarity, we list here again the susceptibility measurements for soil samples taken at two sites on Kaho'olawe.

Table 3 lists measurements of the magnetic susceptibility for soil samples at Seagull and Lua Kakika sites on Kaho'Olawe. Three separate samples were measured from each bag of soil. The mean of the measurements is listed.

(a) Seagull Site - Magnetic Susceptibility ($\times 10^{-5}$ SI)

| Sample | Low Frequency (0.46 kHz) | High Frequency (4.6 kHz) | % Frequency Effect |
|-----------------|-----------------------------|-----------------------------|-----------------------|
| 7462-2728A-6" | 3554 | 3311 | 7.0 |
| 7462-2728A-24" | 3022 | 2771 | 8.2 |
| 7462-2728B-6" | 1046 | 1001 | 4.3 |
| 7468-2734AP-6" | 1726 | 1630 | 5.6 |
| 7468-2734AP-18" | 1529 | 1448 | 5.3 |
| 7468-2734BP-12" | 2807 | 2634 | 6.2 |
| 7468-2734BP-24" | 1920 | 1807 | 5.9 |
| 7468-2734AB-6" | 845 | 805 | 4.6 |
| 7468-2734BB-8" | 1795 | 1707 | 4.9 |

(b) Lua Kakika Site - Magnetic Susceptibility ($\times 10^{-5}$ SI)

| Sample | Low Frequency (0.46 kHz) | High Frequency (4.6 kHz) | % Frequency Effect |
|-----------------|-----------------------------|-----------------------------|-----------------------|
| 7537-2754AP-6" | 2355 | 2249 | 4.5 |
| 7537-2754AP-18" | 2227 | 2134 | 4.2 |
| 7537-2754BP-12" | 1461 | 1383 | 5.4 |
| 7537-2754BP-24" | 1497 | 1411 | 5.8 |
| 7537-2754AB-6" | 2475 | 2431 | 1.8 |
| 7537-2754B-12" | 1394 | 1334 | 4.3 |

These measurements provide us with the real part of the complex susceptibility at two frequencies. Given this limited information of the soil's magnetic characteristics, we need to make some assumptions in generating a susceptibility model. First, we assume that the two measuring frequencies are within the frequency range where the inphase component decreases linearly with the logarithm of frequency ($\tau_2^{-1} \ll \omega \ll \tau_1^{-1}$). Second, we assume that all the

frequencies of interest fall within this range of frequencies. With these two assumptions, we can model the real part of the susceptibility as a straight line. By manipulating equation 1 we can show that for $\tau_2 \gg \tau_1$ the slope of the in-phase component is related to the quadrature component by

$$\text{Slope} = \left[\frac{\partial \text{Re}(\chi)}{\partial \ln \omega} \right] = \frac{2}{\pi} \text{Im}(\chi(\omega)) = -\frac{\chi_o}{\ln(\tau_2/\tau_1)} \quad (11)$$

This relationship has also been derived without the use of equation (8) (Mullins and Tite, 1974), and has been observed in complex susceptibility measurements by Dabas et al. (1992). Therefore, by determining the slope of the inphase component from the susceptibility measurements, we can immediately estimate the quadrature component. The susceptibility model of Figure 13 was constructed using susceptibility measurements of sample 7462-2728A-6 (Table 3). In 1D earth modeling that follows, one of the layered earth models considered will use this magnetic susceptibility model to represent the susceptibility for the top layer of soil.

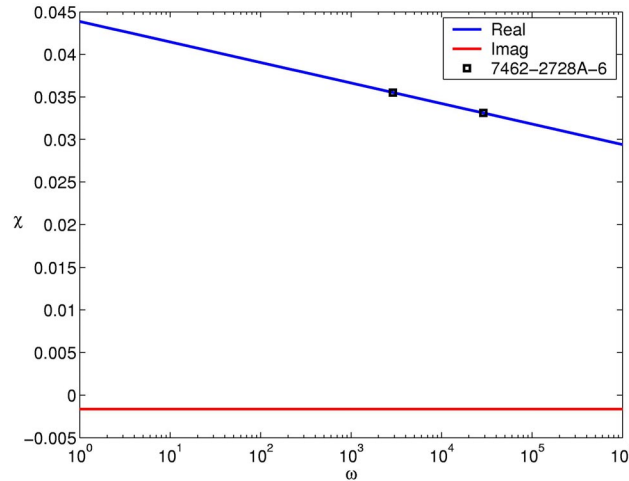


Figure 13: A magnetic susceptibility model constructed for soil sample 7463-2726A-6 from Seagull Site at Kaho’olawe, Hawaii.

4.3 Electromagnetic Response of a 1-D Layered Magnetic Earth

Forward modelling in 1D is solved in the frequency domain in the standard propagation matrix formalism (Farquharson et al., 2001). Let us consider a circular transmitter loop of radius α , carrying a current I , and at a height h above a 1-D layered earth. At an observation point z above the ground and a radial distance ρ from the axis of circular transmitter loop, the vertical component H_z and the radial component H_ρ of the \mathbf{H} -field are

$$H_\rho(\omega) = \frac{Ia}{2} \int_0^\infty \left[e^{-u_o(z+h)} - \frac{P_{21}}{P_{11}} e^{u_o(z-h)} \right] \lambda J_1(\lambda a) J_1(\lambda \rho) d\lambda \quad (12)$$

$$H_z(\omega) = \frac{Ia}{2} \int_0^\infty \left[e^{-u_o(z+h)} + \frac{P_{21}}{P_{11}} e^{u_o(z-h)} \right] \frac{\lambda^2}{u_o} J_1(\lambda a) J_0(\lambda \rho) d\lambda \quad (13)$$

where $u_o = \sqrt{\lambda^2 - k_o^2}$, k_o is the wave number of the air, and J_0 and J_1 are the zeroth and first order Bessel functions, respectively. P_{21} and P_{11} are elements of the matrix \mathbf{P} :

$$\mathbf{P} = \mathbf{M}_1 \prod_{j=2}^m \mathbf{M}_2 \quad (14)$$

where

$$\mathbf{M}_1 = \begin{bmatrix} \frac{1}{2} \left(1 + \frac{\mu_0 \mu_1}{\mu_1 \mu_0} \right) & \frac{1}{2} \left(1 + \frac{\mu_0 \mu_1}{\mu_1 \mu_0} \right) \\ \frac{1}{2} \left(1 + \frac{\mu_0 \mu_1}{\mu_1 \mu_0} \right) & \frac{1}{2} \left(1 + \frac{\mu_0 \mu_1}{\mu_1 \mu_0} \right) \end{bmatrix} \quad (15)$$

$$\mathbf{M}_1 = \begin{bmatrix} \frac{1}{2} \left(1 + \frac{\mu_j - 1 \mu_1}{\mu_j \mu_j - 1} \right) & \frac{1}{2} \left(1 - \frac{\mu_j 1 \mu_j}{\mu_j \mu_j - 1} \right) \\ \frac{1}{2} \left(1 - \frac{\mu_j - 1 \mu_j}{\mu_j \mu_j - 1} \right) e^{-2u_{j-1} t_{j-1}} & \frac{1}{2} \left(1 + \frac{\mu_j - 1 \mu_j}{\mu_j \mu_j - 1} \right) e^{-2u_{j-1} t_{j-1}} \end{bmatrix} \quad (16)$$

The thickness of the j^{th} layer is t_j , and μ_j is the magnetic permeability of the layer.

To determine the fields at the center of the transmitter loop, we can simply set $\rho = 0$ and set $z = -h$. These substitutions give

$$H_\rho(\omega) = 0 \quad (17)$$

$$H_z(\omega) = \frac{Ia}{2} \int_0^\infty \left[1 + \frac{P_{21}}{P_{11}} e^{-2u_o h} \right] \frac{\lambda^2}{u_o} J_1(\lambda a) (\lambda a) d\lambda \quad (18)$$

Therefore, as the symmetry of the 1-D would also suggest, there is no horizontal component to the \mathbf{H} -field response at the center of the transmitter loop. This is an important point because it shows, for the situation where the fields are measured along the axis of the transmitter loop, that the effects of magnetic susceptibility will appear only in the vertical component. This feature will be exploited later when processing electromagnetic data.

The time domain solution is obtained by calculating Fourier transformations of the frequency response for a causal step turn-off (Newman et al., 1986):

$$\frac{\partial h(t)}{\partial t} = -\frac{2}{\pi} \int_0^\infty \text{Re}[H(\omega)] \cos(\omega t) d\omega \quad (19)$$

$$\frac{\partial h(t)}{\partial t} = -\frac{2}{\pi} \int_0^\infty \text{Im}[H(\omega)] \sin(\omega t) d\omega \quad (20)$$

$$h(t) = -\frac{2}{\pi} \int_0^\infty \frac{\text{Im}[H(\omega)]}{\omega} \cos(\omega t) d\omega \quad (21)$$

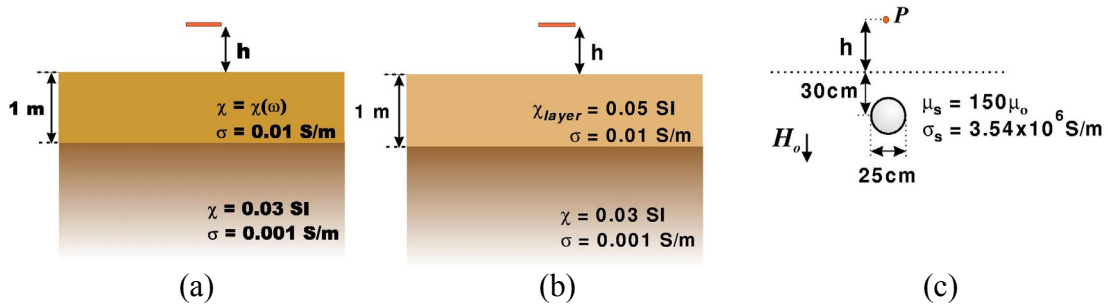


Figure 14 Three example models. Panel (a) shows a two-layer model with frequency dependent magnetic susceptibility $\chi(\omega)$ in the top layer. Panel (b) show a Two layer model with static magnetic susceptibility. Panel (c) shows conductive and permeable metal sphere. Material parameters are chosen to match steel.

Let us consider a pair of two-layer models. The first, shown in Figure 14(a), consists of a 1 m thick top layer with a conductivity of $\sigma = 0.01$ S/m and a frequency dependent complex susceptibility defined by Figure 13. The second two-layer model, shown in Figure 3(b), has a static real susceptibility of $\chi = 0.05$ SI in the top layer. Both models have a basement conductivity of $\sigma = 0.001$ S/m and a static susceptibility of $\chi = 0.03$ SI. The calculated responses of this two-layer model will be compared to the response of a conductive and permeable sphere with the approximate material properties of steel ($\mu = 150\mu_0$, $\sigma = 3.54 \times 10^6$ S/m), a diameter of 25 cm, and buried at a depth of 30 cm. The sphere response will be approximated using the solution outlined by Ward (1959) for a sphere in a uniform field in a whole space.

Figure 15(a) shows the modeled frequency response for the two-layer models. When plotting the responses at the chosen axis ranges, the results for the static, real susceptible model and the model with complex susceptibility look similar. Subtle, but important, differences become apparent when focusing the plot on the lower frequency range. Figure 15(b) shows that the real part of the \mathbf{H} -field has a line of negative slope. The effect of the frequency dependent layer on the quadrature component becomes evident when plotting the logarithm of the quadrature component (Figure 15(c)). The effect of these differences on the time domain signature is shown in Figure 16(a).

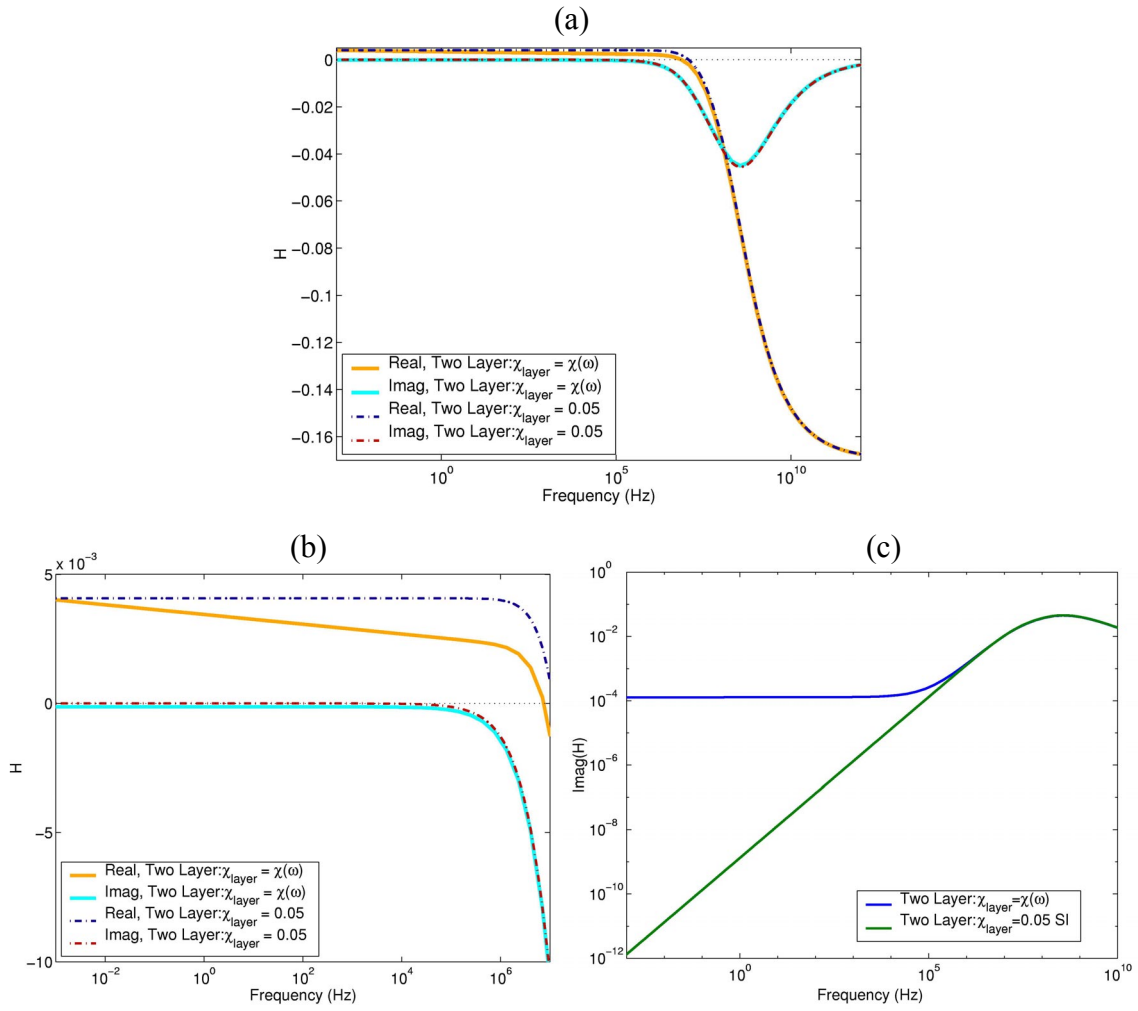


Figure 15 Forward modelled frequency domain electromagnetic responses for the two layer model. Panel (a): the solid lines represent the response of the two layer model with frequency dependent susceptibility (Fig. 14(a)) and dashed lines represent the two layer model with real, static susceptibility (Fig. 14(b)). Panel (b) is the Frequency domain response of the two layer model between 10^{-3} and 10^7 Hz. Panel (c) is the imaginary part of \mathbf{H} -Field for the two layer model with frequency dependent susceptibility and with real static susceptibility.

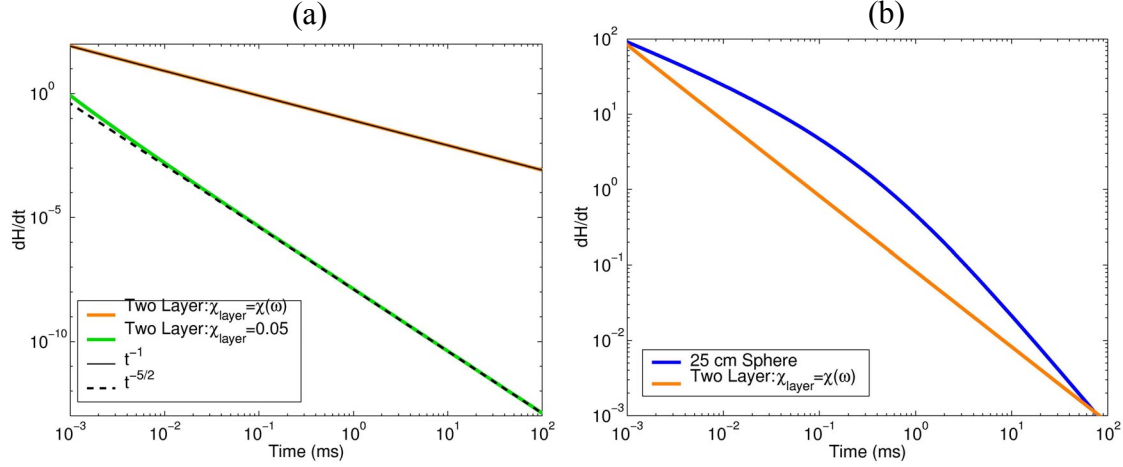


Figure 16 Forward modelled electromagnetic responses for the two layer model and the sphere model. Panel (a) is Time domain responses of the two layer models. The model with frequency dependent susceptibility follows the t^{-1} response while the model with only static, real susceptibility follows a $t^{-5/2}$ decay. Panel (b) is the Time domain responses of the steel sphere and the two-layer model with frequency dependent susceptibility.

We see that the two layer model with complex, frequency dependent susceptibility produces a t^{-1} response, while the two-layer model with static real susceptibility follows a $t^{-5/2}$ decay. For the time range of the Geonics EM63 (approximately 0.1 ms to 25 ms) it is clear that the response of the real, static susceptibility distribution produces a much weaker response than when the model contains the complex, frequency dependent susceptibility layer. Figure 15(d) shows the response of the sphere model is much larger than the TEM response of the model with only static, real susceptibility. However the TEM response for the model with complex susceptibility becomes comparable at early and late times.

The t^{-1} response only occurs for a step function primary field. To take into account the finite length of the inducing field we can convolve the solution with the transmitter current (Asten, 1987). The full waveform convolution is

$$h_R(t) = \int_0^{\infty} h(t')h_T(t-t')dt' \quad (22)$$

where the $h_R(t)$ is the receiver waveform and $h_T(t)$ is the transmitter waveform.

5. The Effect of Magnetic Soils on the Recovery of Dipole Parameters and its removal

In this section we consider the effect the magnetic soils have on our ability to recover the representative dipole parameters of a buried target from a 3-component time domain sensor data.

5.1 Generation of Synthetic TEM Data

Although 3-component sensors have been developed by Geonics Inc. (EM61-3D) and Zonge Engineering (NanoTEM), testing of either sensor has been limited. Field data, in particular data acquired over magnetic soils, are not readily available. Therefore, to investigate the effects of the magnetic soils we must generate synthetic data sets. We assume that the secondary field is a linear sum of the response of the buried metallic target, the response of the magnetic soil and Gaussian noise. We use the conclusion, arrived at earlier, that the magnetic soils affect only the vertical component of the receiver if the receiver is on the axis of the transmitter.

The buried target response is calculated by using the decaying two-dipole approximation outlined in Pasion and Oldenburg (2001a). The response of a compact buried target can be approximated by a 13 element model vector:

$$\bar{m} = (X, Y, d, \theta, \phi, \kappa_1, \alpha_1, \beta_1, \gamma_1, \kappa_2, \alpha_2, \beta_2, \gamma_2)^T, \quad (23)$$

where (X, Y) is the target location, d is the depth below the surface, and θ and ϕ define the target orientation, $\kappa_1, \alpha_1, \beta_1, \gamma_1$ define the decay characteristic of a dipole oriented parallel to the axis of symmetry of the target, $\kappa_2, \alpha_2, \beta_2, \gamma_2$ define the decay characteristic of a dipole oriented perpendicular to the axis of symmetry of the target. Verification of this model, as well as appropriate parameters for different UXO and scrap targets, are reported in Pasion and Oldenburg (2001b). For the examples in this paper, we will forward model the response for the stokes mortar of Figure 4.



| Dipole 1 | | Dipole 2 | |
|------------|------|------------|-------|
| k_1 | 43.9 | k_2 | 4.9 |
| α_1 | 0.02 | α_2 | 0.001 |
| β_1 | 0.73 | β_2 | 1.09 |
| γ_1 | 9.1 | γ_2 | 10.8 |

Figure 17: Photo of a Stokes mortar and its dipole decay constants.

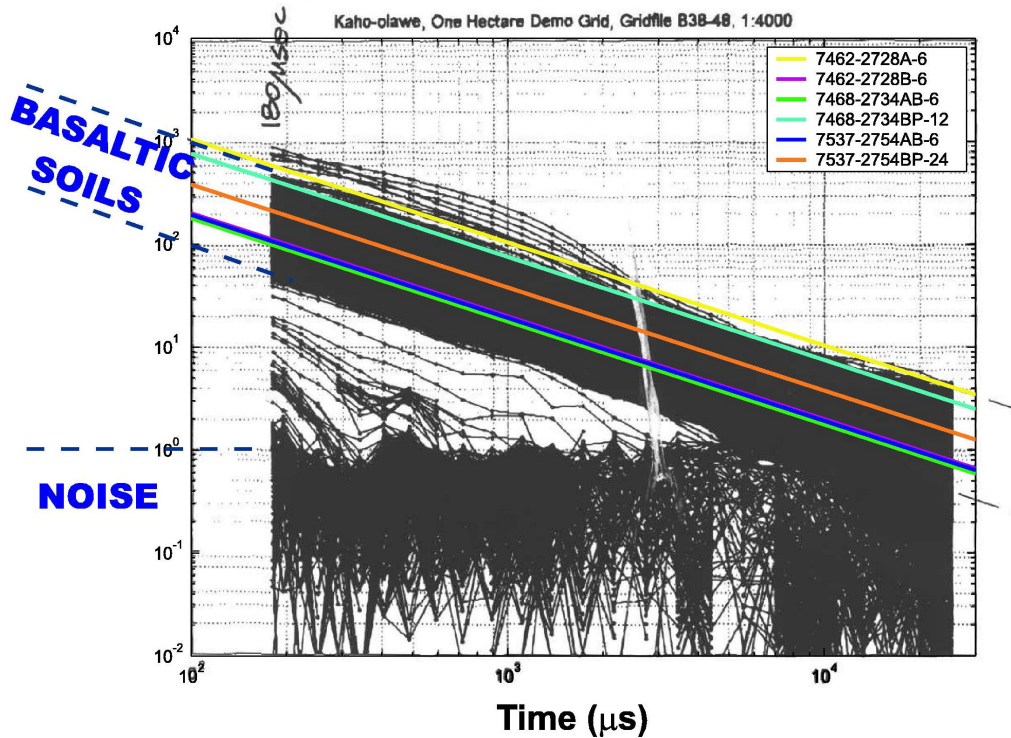


Figure 18 Geonics EM63 TEM data collected on Kaho'olawe island. Overlaid on the data are responses of two layer models. The top layer susceptibility model is generated using measured susceptibilities from Table 3 and eq. (8).

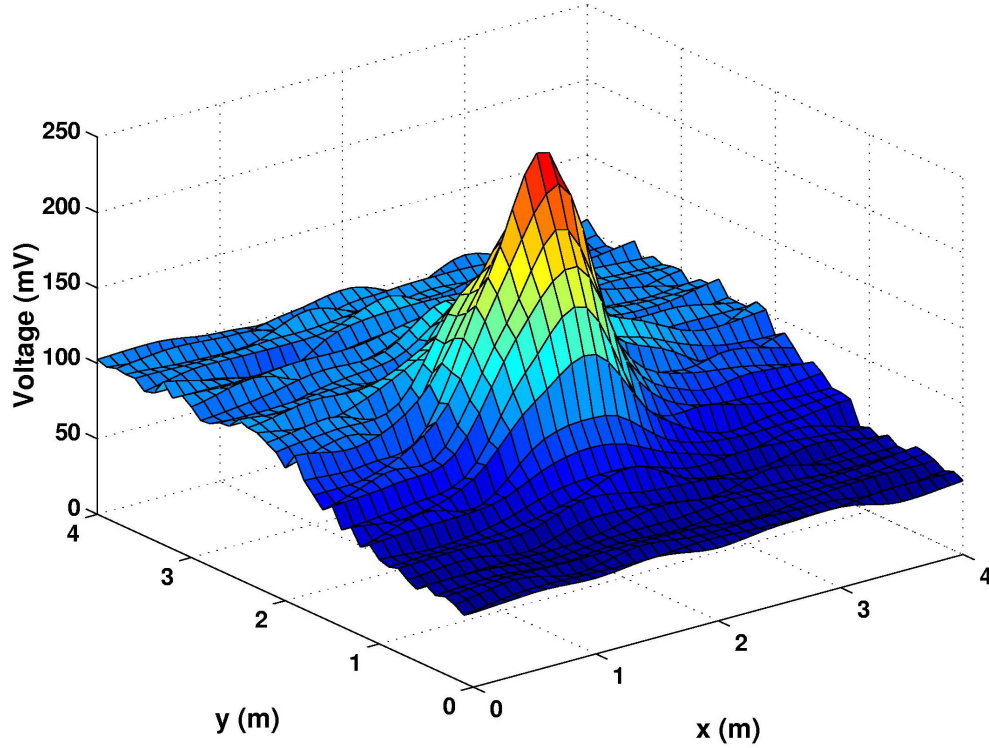


Figure 19 First time channel of synthetic data generated for a Stokes mortar buried in a two-layer background.

Data will be generated for a 4 m X 4 m survey area, with lines collected at 0.5 m separation, and soundings collected every 10 cm along each line. The mortar is placed at $(X, Y) = (2\text{m}, 2\text{m})$ and at a depth of 40 cm. The target is oriented such that $(\theta, \phi) = (30 \text{ degrees}, 70 \text{ degrees})$.

To model horizontal variation of magnetic soils we assume that the magnetic soil response is

$$F^{soil} = A(x,y) \hat{t}^1, \quad (24)$$

where the amplitude $A(x,y)$ can vary across the survey area. Figure 18 contains data collected on Kaho'olawe with a Geonics EM63 TEM sensor. From the plotted decay curves, we see that the basaltic soils produces a response of approximately 100mV at the first time channel (180 μsec). The amplitude $A(x,y)$ is defined as

$$A(x, y) = \frac{k}{2} \left[1 + \tanh \left(2 \left(x - \frac{3}{2} \right) \right) \right] \quad (25)$$

where k is chosen such that at the first time channel the background soil response is 50 mV at $Y=0$ m and increases to 100 mV at $Y=4$ m. Finally noise ε , with a standard deviation of 5% of the data plus 0.5 mV, are added to the sum of the basalt response and the dipole response. Figure 19 plots the synthetic data at $t=180 \mu\text{sec}$.

5.2 Pre-processing Using Horizontal Components of Field

As our modelling suggests, the presence of magnetic soils will produce a t^{-1} signal in the vertical component of the measured secondary field. The difficulty in removing this signal lies in identifying whether the measured response arises only from the soil or from a combination of soil and a metallic target. The absence of the soil signal in the horizontal components suggest that they can be used as part of a pre-processing step to help determine where and how we should attempt to remove the soil signal in the vertical component. One possible (and simple) way of doing this would be the following:

1. Calculate the horizontal component of the data at the first time channel:

$$d^h(t_1) = \sqrt{d_x^2(t_1) + d_y^2(t_1)} .$$

2. At each sounding, if d^h is less than some threshold value (e.g. $d^h < 2\text{mV}$) then identify this station as unlikely to contain signal from a target. We can proceed to fit $A t^{-1}$ to the data at this station and subtract from the data.
3. At soundings where d^h is greater than the threshold, we can then subtract $A(\text{dagger}) t^{-1}$ where $A(\text{dagger})$ is determined from interpolation of the A values from the previous step.

The synthetic data were inverted for the 13 parameters listed in eq. (23). These parameters were obtained by minimizing a least squares objective function. Three data sets we considered are: (1) Stokes mortar without magnetic soil response, (2) Stokes mortar with the magnetic soils noise model, and (3) Stokes mortar with a magnetic soil background, where the data has been pre-processed using the horizontal components to remove the response from the vertical components. The results of inverting the data sets are shown in Table 4.

Table 4 Inversion results for a Stokes mortar buried in a background of magnetic soils.

| | Real Params | No Basalt | W/Basalt Model | Basalt Removed |
|------------|-------------|-----------|----------------|----------------|
| X | 2 | 2.00 | 2.08 | 2.02 |
| Y | 2 | 2.00 | 2.00 | 1.98 |
| D | 0.4 | 0.40 | 0.58 | 0.42 |
| θ | 30 | 29.9 | 41.1 | 38.2 |
| ϕ | 70 | 70.0 | 74.2 | 69.3 |
| k_1 | 43.9 | 45.35 | 125.69 | 47.45 |
| α_1 | 0.02 | 0.02 | 0.00 | 0.02 |
| β_1 | 0.73 | 0.73 | 0.71 | 0.72 |
| γ_1 | 9.1 | 9.17 | 29.31 | 9.04 |
| K_2 | 4.9 | 4.96 | 26.05 | 6.62 |
| α_2 | 0.001 | 0.02 | 0.00 | 0.02 |
| β_2 | 1.09 | 1.16 | 0.80 | 1.04 |
| γ_2 | 10.8 | 12.69 | 29.23 | 15.06 |

The inversion was successful in recovering the location, orientation, and dipole parameters without the magnetic soil signal, and when the data was pre-processed as described in the previous section. The inversion of the unprocessed data set that contained the magnetic soil signal was unable to accurately recover the dipole decay parameters.

5.4 Summary

Electromagnetic sensor data acquired in the presence of magnetic soils have a characteristic $\partial H / \partial t$ decay of t^{-1} . This t^{-1} decay can be derived by assuming the soil consists of magnetic particles with a uniform distribution of decay times. This assumption leads to a representation of the magnetic susceptibility as a frequency dependent, complex quantity. 1D forward modeling of this susceptibility model reveals that the horizontal components of data measured along the axis of a transmitter loop are not sensitive to magnetic soils provided that the subsurface properties can be adequately represented by a 1D layered model. As a consequence, when inverting the three component sensor data collected over a target buried in magnetic soil, the information provided by the horizontal components of data may: (1) improve detection, (2) be exploited in developing processing routines to aid in the removal of the magnetic soil response in

the vertical component of data, and (3) help constrain the inversion to more reliably recover dipole model parameters.

6. Conclusions

We have examined the effect of magnetic soil on static magnetic method and time-domain electromagnetic method used in the UXO discrimination problems. We have developed quantitative understanding of the effect and proposed simple processing techniques to alleviate the soil effect and increase the reliability of the model parameters inverted from both data sets used in discrimination.

In magnetic method, spatial variation of the static magnetic susceptibility is modeled using a correlated random process in 3D. The spectral properties of the random process is estimated from the field data observed at Kaho'olawe clearance site and then used in the simulations. Numerical modeling and inversion provide clear indication of the condition under which the magnetic soil can completely mask UXO response. We have found that Wiener filter is effective in suppressing the soil response as a preprocessing tool. However, its effectiveness depends critically upon our ability to estimate the power spectrum of the soil response. In general, the filtered result will be useful for detection purposes, but it may not be sufficient for discrimination purposes. Reliable estimation of the power spectrum of soil response depends on good characterization of spatial variation of susceptibility at the clearance site. Further work using field data at sites with strong magnetic soil is therefore required.

In time-domain electromagnetic method, the frequency dependent susceptibility is modeled using a complex susceptibility with a broad range of relaxation times. Electromagnetic sensor data acquired in the presence of such magnetic soils have a characteristic $\partial H / \partial t$ decay of t^{-1} . This provides a theoretic understanding of the t^{-1} decay observed in the field when highly magnetic soil is present. 1D forward modeling of this susceptibility model reveals that the horizontal components of data measured along the axis of a transmitter loop are not sensitive to magnetic soils provided that the subsurface properties can be adequately represented by a 1D layered model. As a consequence, when inverting the three component sensor data collected over a target buried in magnetic soil, the information provided by the horizontal components of

data may be used to improve detection and help preprocess the vertical component to alleviate the soil response, and ultimately improve the inversion results. Similar to magnetic method, further investigation at field sites is required to determine the relaxation parameters of the complex susceptibility and its spatial distribution.

7. Acknowledgements

This research was funded by SERDP through SEED project UX-1285. We thank Dr. Anne Andrews and Mr. Jeffrey Fairbanks from SERDP for their constant help during the project. We also thank Dr. Dwain Butler from the Engineer Research and Development Center for the magnetic susceptibility measurements of soil samples from Kaho'olawe, Hawaii.

8. References

- Asten, M. W., 1987, Full transmitter waveform transient electromagnetic modeling and inversion for soundings over coal measures: *Geophysics*, **47**, 1315-1324.
- Billings, S. D., Pasion, L. R., and Oldenburg, D.W., 2002, UXO discrimination and identification using magnetometry, *Proceedings of SAGEEP*.
- Blakely, R. J., 1995, *Potential theory and its application in gravity and magnetic exploration*, Cambridge University Press.
- Easley, D. H., Borgman, L. E. and Shive, P. N., 1990, Geostatistical simulation for geophysical applications - Part I: Simulation: *Geophysics*, **55**, 1435-1440.
- Cespedes, E.R., 2001, demonstration of advanced unexploded ordnance detection and discrimination technologies at Kaho'olawe, Hawaii: *Proceedings of Partners in Environmental Technology Technical Symposium and Workshop*, Washington, D.C.
- Dabas, M., Jolivet, J., and Tabbagh, Al, 1992, Magnetic susceptibility and viscosity of soils in a weak time varying field: *Geophysical Journal International*, **108**, 101-109.
- Farquharson, C.G., Oldenburg, D.W., and Routh, P. S., 2001, Simultaneous one-dimensional inversion of loop-loop electromagnetic data for both magnetic susceptibility and electrical conductivity, submitted to *Geophysics*.
- Mullins, C.E. and Tite, M.S., 1974, Magnetic susceptibility and frequency dependence of susceptibility in single-domain assemblies of magnetite and maghemite: *J. Geophys. Res*, **78**, 804-809.

Newman, G.A., Hohmann, G.W., and Anderson, W.L., 1986, Transient electromagnetic response of a three-dimensional body in a layered earth: *Geophysics*, **51**, no.8, 1608-1627.

Olhoeft, G.R. and Strangway, D.W., 1974, Magnetic relaxation and the electromagnetic response parameter: *Geophysics*, **39**, no.3, 302-311.

Parsons Engineering and UXB International Inc., 1998, Cleanup Plan: UXO Clearance Project, Kaho'olawe Island Reserve, Hawaii. Prepared for Naval Facilities Engineering Command Pacific Division.

Pasion, L.R. and Oldenburg, D.W., 2001a, A discrimination algorithm for UXO using time domain electromagnetics: *Journal of Engineering and Environmental Geophysics*, **6**, no.2, 91-102.

Pasion, L.R. and Oldenburg, D.W., 2001b, Locating and characterizing unexploded ordnance using time domain electromagnetic induction, Technical Report, ERDC/GSL TR-01-10, U.S. Army Research and Development Center, Vicksburg, MS.

Lee, T., 1983, The Effect of a superparamagnetic layer on the transient electromagnetic response of a ground: *Geophysical Prospecting*, **32**, 480-496.

Li, Y., and Oldenburg, D. W., 1996, 3D inversion of magnetic data, *Geophysics*, **61**, 394-408.

Scollar, I., Tabbagh, A., Hesse, A., and Herzog, I., 1990. Archaeological prospecting and remote Sensing. Cambridge University Press, Cambridge.

Sharma, P. V., 1966, Rapid computation of magnetic anomalies and demagnetization effects caused by bodies of arbitrary shape, *Pure Appl. Geophys.* **64**, 89-109.

Shive, P. N., Lowry, T., Easley, D. H. and Borgman, L. E., 1990, Geostatistical simulation for geophysical applications - Part II: Geophysical: *Geophysics*, **55**, 1441-1446.

Stearns, H. T. 1940. Geology of ground water resources on the Islands of Lanai and Kaho'olawe, Hawaii, Bulletin 6. Hawaii Division of Hydrography, Honolulu, Hawaii.

Ward, S.H., 1959, Unique determination of conductivity, susceptibility, size, and depth in multifrequency electromagnetic exploration: *Geophysics*, **24**, no.3, 531-546.

Ward, S.H., and Hohmann, G.W., 1991, Electromagnetic Theory for Geophysical Applications, *in* Nabighian, M.N., Ed., *Electromagnetic Methods In Applied Geophysics: Society of Exploration Geophysicists, Volume 1, Theory*, 131-311.

Wiener, N., 1949, Extrapolation, interpolation, and smoothing of stationary time series, Cambridge, MIT Press.